Pflugers Arch - Eur J Physiol (2006) 452: 175–187
DOI 10.1007/s00424-005-0019-4

CELLULAR NEUROPHYSIOLOGY

A. Pantazis · P. Keegan · M. Postma · C. J. Schwiening

# The effect of neuronal morphology and membrane-permeant weak acid and base on the dissipation of depolarization-induced pH gradients in snail neurons

Received: 22 June 2005 / Revised: 15 September 2005 / Accepted: 26 October 2005 / Published online: 10 December 2005


**Abstract** Neuronal depolarization causes larger intracellular pH ($pH_i$) shifts in axonal and dendritic regions than in the cell body. In this paper, we present evidence relating the time for collapse of these gradients to neuronal morphology. We have used ratiometric $pH_i$ measurements using 8-hydroxypyrene-1,3,6-trisulfonic acid (HPTS) in whole-cell patch-clamped snail neurons to study the collapse of longitudinal pH gradients. Using depolarization to open voltage-gated proton channels, we produced alkaline $pH_i$ microdomains. In the absence of added mobile buffers, facilitated $H^+$ diffusion down the length of the axon plays a critical role in determining $pH_i$ microdomain lifetime, with axons of ~100 μm allowing pH differences to be maintained for >60 s. An application of mobile, membrane-permeant pH buffers accelerated the collapse of the alkaline-pH gradients but, even at 30 mM, was unable to abolish them. Modeling of the $pH_i$ dynamics showed that both the relatively weak effect of the weak acid/base on the peak size of the pH gradient and the accelerated collapse of the pH gradient could be due to the time taken for equilibration of the weak acid and base across the cell. We propose that appropriate weak acid/base mixes may provide a simple method for studying the role of local $pH_i$ signals without perturbing steady-state $pH_i$. Furthermore, an extrapolation of our in vitro data to longer and thinner neuronal structures found in the mammalian nervous system suggests that dendritic and axonal $pH_i$ are likely to be dominated by local $pH_i$-regulating mechanisms rather than simply following the soma $pH_i$.

**Keywords** Intracellular pH · Proton channels · Fluorescence imaging · Neurones

A. Pantazis · M. Postma
Department of Anatomy,
University of Cambridge,
Downing Street,
Cambridge CB2 3DY, UK

P. Keegan · C. J. Schwiening (✉)
Department of Physiology,
University of Cambridge,
Downing Street,
Cambridge CB2 3EG, UK
e-mail: cjs30@cam.ac.uk
Tel.: +44-1223-333827
Fax: +44-1223-333840

## Introduction

Electrical activity of neurons opens voltage-gated channels, allowing an influx of calcium down its electrochemical gradient. In snail neurons, if the depolarization is sufficiently large, this may also be accompanied by the opening of proton channels. The rise in intracellular calcium stimulates a number of processes that lead to cytoplasmic acidification [1–3] whilst the efflux of $H^+$, through proton channels, leads to an intracellular alkalinization. Since the surface area to volume ratio of subcellular regions varies, even uniform transmembrane acid fluxes can lead to the development of intracellular pH ($pH_i$) gradients. Such intracellular pH gradients were first demonstrated in snail neurons [4]. These activity-dependent, intracellular pH shifts were found to be significantly larger in neuronal processes than in the cell body and persisted for seconds [4, 5]. Although there is a considerable body of literature on proton buffering and diffusion [6–11], there is no experimental evidence that directly addresses the effect of neuronal morphology on the lifetime of $pH_i$ gradients or the effect of exogenously applied weak acids and bases upon them. Similarly, although mathematical diffusional models for $pH_i$ microdomain kinetics have been published [12], there is little experimental, morphological, neuronal data to validate them.

In this paper, we have tested whether or not neuronal $pH_i$ is uniform under resting conditions [13–16] and investigated experimentally the effect of neuronal morphology and mobile pH buffers on the time course of the local $pH_i$ signals [12]. We have used snail neurons in this study as they are experimentally tractable and have well-

characterized pH-regulating mechanisms [3, 6, 17], including voltage-gated proton channels that allow very rapid and non-uniform changes in $pH_i$ [4, 18].

The pH of axons and dendrites is determined by two main sets of processes: local transmembrane acid equivalent fluxes and cytoplasmic acid equivalent diffusion. Transmembrane fluxes can both perturb [3, 19] and re-equilibrate $pH_i$ [20, 21]. However, passive diffusion of acid equivalents can only act to dissipate $pH_i$ gradients. Acid equivalents cross the plasma membrane on three main transporters, the $Ca^{2+}$–$H^+$ pump (PMCA or $Ca^{2+}$-pump) [3], the $Na^+$-dependent $Cl^-$–$HCO_3^-$ exchanger [20] and the $Na^+$–$H^+$ exchanger [17]. To investigate the uniformity of *resting* $pH_i$, we measured regional pH ratiometrically under conditions designed to reduce the activity of these acid equivalent transporters. This was achieved by preventing the opening (by holding the membrane potential at −60 mV) of voltage-gated calcium channels which would otherwise lead to increased $Ca^{2+}$–$H^+$ pump activity and by keeping external $HCO_3^-$ low (~100 μM through equilibration with ambient $CO_2$) to reduce $Na^+$-dependent $Cl^-$–$HCO_3^-$ exchanger activity. However, we did not block the $Na^+$–$H^+$ exchanger [22] to allow for some acid extrusion and thereby minimize acidosis caused by calcium-dependent acid loading mechanisms such as the $Ca^{2+}$:$H^+$ pump and mitochondria. To investigate the effect of neuronal morphology on the collapse of activity-dependent pH shifts, we again used conditions designed to minimize transmembrane acid fluxes. To do this we kept $HCO_3^-$ low and used voltage-gated proton channels [18] to evoke alkaline pH shifts, which do not increase the activity of any known snail $pH_i$-regulating mechanisms [6]. We then analyzed the rate of collapse of the depolarization-evoked $pH_i$ shifts in neurons with differing cellular dimensions [4]. Since the alkaline load terminates immediately on repolarization, such $pH_i$ recoveries are governed only by local proton mobility and residual $pH_i$ regulation. To test the effect of proton mobility and open-system $H^+$ buffering on the lifetime of regional pH transients, we avoided the use of the $CO_2/HCO_3^-$ pH buffer which would activate pH-regulating mechanisms. Instead, we used external application of membrane-permeant weak acids and bases. This mixture [23] has the advantage of neither largely altering resting $pH_i$, activating pH-regulating mechanisms, requiring carbonic anhydrase activity nor requiring specialized gas mixtures. Avoiding alterations in $pH_i$ is of critical importance since $H^+$ diffusion is known to be critically dependent upon $pH_i$ [8, 24].

Using these techniques, we have found that, with the majority of the pH-regulating mechanisms blocked, resting $pH_i$ is uniform. We also show that axonal morphology and proton mobility are critical in determining regional pH microdomain lifetime. Weak acids and bases have little effect on the peak size of the pH gradients, but they speed the collapse of the gradient. Their effect on the pH gradient collapse is complex and occurs through both facilitated intracellular $H^+$ diffusion and open-system $H^+$ buffering [25]. A small portion of this work has been published in abstract form [26].

## Materials and methods

### Neuronal isolation

The isolation procedure was that described by Schwiening and Willoughby [4]. Briefly, sub-esophageal ganglia were removed from common garden snails, *Helix aspersa*, and were incubated in 1 ml of 1 mg $ml^{-1}$ protease type XIV in pH 7.5 snail Ringer for 1 h at 33°C. They were then washed in snail Ringer and agitated by repeatedly passing the tissue through a fire-polished plastic Pasteur pipette (internal tip diameter ~1.5 mm). This stage of the isolation process required some care since insufficient agitation typically yielded too few single neurons, whilst too much yielded spherical neurons with no visible axon. An aliquot of cells (1 ml) was pipetted into the superfusion chamber, which was mounted on the stage of an inverted microscope.

### Electrophysiology

Patch pipettes (tip diameter ~1.5 μm) were pulled from 1 mm diameter unfilamented borosilicate glass (GC100, Clark Electromedical, UK). The pipette filler solution contained the pH-sensitive fluorescent dye 8-hydroxypyrene-1,3,6-trisulfonic acid (HPTS). A cell with an axonal projection >30 μm was selected and patched [4] using mild negative pressure. The potential of the patch was set to −60 mV, and after a seal of >1 GΩ was achieved, a stronger suck was applied to the patch-pipette to obtain the whole-cell configuration. The voltage-clamp gain, capacitance compensation and bridging were adjusted to maximize voltage control. Errors associated with series resistance were minimized by the inclusion of the $K^+$ channel blocker $Cs^+$ in the patch pipette. Approximately 3 min was then allowed for the dye fluorescence in the axonal process to stabilize before the recording was started. The patch-clamp amplifier was an Axoclamp 2B (0.1 gain headstage, Axon Instruments, USA) and data were recorded using a CED 1401 digitiser and Spike2 software (Cambridge Electronic Design, UK).

### Fluorescence measurements

pH measurements were derived from ratiometric recordings of regional HPTS fluorescence. Cells were illuminated with alternating (10 Hz) 458- and 380-nm light (±15 nm) using a computer-controlled monochromator (Cairn, UK) on a Nikon Diaphot 300 inverted microscope with a ×40 Fluor (NA 0.85) air objective. Regional (25-μm diameter) fluorescence (>510 nm) was collected from an image plane using two controllable, infrared backlit fibre-optics (Cairn, UK). Fluorescence intensity was detected by photomulti-

plier tubes and recorded synchronously with the electrophysiological data, using Spike2. Background-subtracted fluorescence ratios were calculated after the experiment. Data were smoothed appropriately using a high-frequency, digital, finite impulse response filter in Microsoft Excel. Calibrated pH values were obtained using a standard sigmoidal curve [27]. The calibration parameters (maximum ratio, minimum ratio and $pK_{HPTS}$) were obtained from a series of in vitro calibrations [22] performed at the start of the series of experiments.

All data collection, control of the microfluorimeter and calculation of fluorescence ratios were achieved using custom-made scripts in Spike2.

## Solutions

Trimethylamine (TMA) and propionate (Sigma) were added directly to the snail Ringer (composition in millimolar, mM: 80 NaCl, 4 KCl, 7 $CaCl_2$, 5 $MgCl_2$, 20 HEPES—adjusted to pH 7.5 with NaOH) at the start of each experimental day. The patch-pipette solution contained 110 mM CsCl, 5 mM HEPES and 500 μM HPTS set to pH 7.5 with CsOH. The weak acid/base mixes [23] used to alter proton mobility contained propionate and TMA as detailed in Table 1. The relative concentrations of propionate and TMA were chosen to have little effect on $pH_i$ [28]. However, during the course of the experiments, small adjustments in the mix were made (see Table 1) because the original 10:2 mix generally caused a small alkaline transient. All of the mixes had target steady-state $pH_i$ values within 0.1 pH units of 7.1.

## Calibration artefacts

Although our initial measurements of regional $pH_i$, made ratiometrically with HPTS, suggested a steady-state difference between axonal and soma $pH_i$ (Table 2), this was most likely an artefact of the calibration procedure. The calibration of $pH_i$ relies upon the in vitro measurement of fluorescence of HPTS solutions with known pH. In doing such a calibration, it is important to ensure that the recording conditions, using the calibration solutions, are as close as possible to that of the cellular regions in which the measurements to be calibrated were made. We believe that there are two main ways in which our calibrations may not have been ideal. Firstly, the illumination intensity across the imaging field was not uniform. This is a common problem in fluorescence imaging, which may, to an extent, be overcome by applying a 'shading' mask to the imaged data set. As we were recording fluorescence from only two regions (which were in different positions on the image plane from cell to cell), the construction of such a shading mask would have been difficult. The second problem results from a difference in the focusing of the two wavelengths of the excitation light. The result of such distortions is to produce slightly different ratios for the same pH solution depending upon either its location within the imaging field or its *z*-plane thickness. To overcome this, a series of calibrations could have been performed with solutions of different thickness. Given that the photometric fluorescence system consisted of two fibre optics which could move in an analog fashion over the image, correction for both of these artefacts would have been very difficult. The extent to which such calibration problems apply to others who have reported steady-state pH gradients [see Discussion in 14, 15, 29] is unclear. Indeed, the apparent $pH_i$ microdomains published by Ro and Carson [16] are almost certainly the result of imaging artefacts. We are confident in our case that such problems, rather than a true steady-state $pH_i$ gradient, underlie our observations of an apparent steady-state $pH_i$ difference. Our apparent steady-state $pH_i$ gradients were unaffected by manoeuvres that we know collapse dynamic $pH_i$ gradients (i.e. mobile buffer application, Fig. 5). Nevertheless, using HPTS ratiometrically, we can calibrate absolute $pH_i$ within ~0.05 pH units, and we can resolve shifts of less than 0.01 pH units.

**Table 1** The concentrations of the seven weak acid/base mix solutions used to alter proton mobility

| Propionate (mM) | TMA (mM) | Calculated steady-state $pH_i$ | Total acid/base concentration (mM) | Experiments (*n*) |
|---|---|---|---|---|
| 1.63 | 0.25 | 7.09 | 1.88 | 5 |
| 3.25 | 0.50 | 7.09 | 3.75 | 5 |
| 7.50 | 1.00 | 7.06 | 8.50 | 6 |
| 10.0 | 2.00 | 7.15 | 12.0 | 1 |
| 15.0 | 2.00 | 7.06 | 17.0 | 4 |
| 20.0 | 2.00 | 7.00 | 22.0 | 5 |
| 30.0 | 4.00 | 7.06 | 34.0 | 2 |

The steady-state $pH_i$ was calculated from Eisner et al. [23] using the formula $pH_i = pH_o - 0.5 \log([Acid]/[Base])$ (where $pH_o$ is the extracellular pH). The final column gives the number of experiments performed with each buffer mix

**Table 2** Apparent mean calibrated steady-state regional intracellular pH values from 23 experiments (mean±SEM)

| | Axon | Soma |
|---|---|---|
| Initial pH | 7.10±0.07 | 7.16±0.06 |
| pH before weak acid/base addition | 7.11±0.04 | 7.14±0.04 |
| pH during weak acid/base superfusion | 7.05±0.03 | 7.10±0.03 |

The values of apparent axonal pH at the beginning of the experiment, axonal pH just before weak acid/base addition and steady-state axonal pH during superfusion with weak acid/base (mean data for total buffer concentrations in the range 1.88–34.0 mM) were significantly more acidic than those in the soma ($P<0.005$)

## Data analysis

Exponentials and straight line functions were fitted in Excel by least squares using the Solver. Exponentials (scalar × $e^{-\text{time}/\tau}$ + constant where τ is the time constant)

were fitted to pH-dependent ratio data after depolarization to +60 mV, rather than calibrated $pH_i$ to avoid inaccuracies associated with regional in vitro calibration [13, 29]. Morphological measurements were made from long-wavelength light (>600 nm) videomicrographs taken during the experiment, using Paint Shop Pro (JASC, USA).

### Statistics

Mean data are presented as mean±SEM unless stated otherwise and $n$ represents the number of cells used. Statistical significance was calculated using either a linear regression $F$-test or a Student's paired two-tailed $t$-test as appropriate. Linear correlations are denoted by $r^2$.

### $pH_i$ gradient modeling parameters

Permeation and one-dimensional diffusion was modeled using a finite volume scheme implemented in C++. The cell membrane was assumed to be permeable only to the uncharged weak acid ($P_{AH}$, 8.7 μm $s^{-1}$ [30]) and weak base ($P_B$ 27.4 μm $s^{-1}$, estimated from [30]). The diffusion coefficients for both the charged and uncharged forms of the weak acid ($D_A$, $D_{AH}$) and base ($D_{BH}$, $D_B$) were assumed to be 700 $\mu m^2$ $s^{-1}$ and that for free protons ($D_H$) was taken as 6,000 $\mu m^2$ $s^{-1}$ [12]. The mobile endogenous buffering ratio ($\beta_{mob}$ expressed as a ratio of free $H^+$ to bound $H^+$) was taken as comprising 15% [8] of the total $H^+$ buffering ($\beta_{tot}$ ~1:47,000 which is equivalent to ~10 mM of $H^+$ per pH unit at pH 7.1 [31]) with a diffusion coefficient of 800 $\mu m^2$ $s^{-1}$($D_{mob}$ [8]). These values yield an apparent proton diffusion coefficient of 120 $\mu m^2$ $s^{-1}$ (cf. 87 $\mu m^2$ $s^{-1}$ in [12]). The axon (length, $L_{axon}$; radius, $R_{axon}$) was modeled as a cylinder divided into 31 sections. The soma was modeled as a single sphere (radius, $R_{soma}$) connected to the cylinder. The diffusional fluxes were calculated by Fick's law, with permeation proportional to the surface-to-volume ratio, permeability and concentration difference. The buffering kinetics was assumed to be fast such that the buffer was always in equilibrium with the prevailing pH [see 12]. The p$K_a$ values of propionate and TMA were 4.8 and 9.2, respectively. At $t$=10 s, proton efflux ($J_H$), proportional to the surface-to-volume ratio, was activated for 1 s such that an alkalinization of ~0.3 pH units was reached in the axon.

### Model equations

The rate equations used to describe the evolution of the free proton concentration ([H]), weak acid concentration ([$A^-$] and [AH]) and weak base concentration ([B] and [$BH^+$]) are:

$$\frac{d[H^+]}{dt} = \frac{1}{\beta_{tot}}\left((D_H + \beta_{mob}D_{mob})\nabla^2[H^+] + r_{sv}j_H - v_A - v_B\right) \quad (1)$$

$$\frac{d[A^-]}{dt} = D_A\nabla^2[A^-] - v_A \quad (2a)$$

$$\frac{d[AH]}{dt} = D_{AH}\nabla^2[AH] + r_{sv}j_{AH} + v_A \quad (2b)$$

$$\frac{d[\mathrm{B}]}{dt} = D_B\nabla^2[B] + r_{sv}j_B - v_B \quad (3a)$$

$$\frac{d[BH^+]}{dt} = D_{BH}\nabla^2[BH^+] + v_B \quad (3b)$$

The surface-to-volume ratio ($r_{sv}$) for the axon is $2/R_{axon}$ and for the soma $3/R_{soma}$. The reaction kinetics ($v_A$, $v_B$) of protonation and deprotonation are:

$$v_A = k_A^{on}[A^-][H^+] - k_A^{off}[AH] \quad (4a)$$

$$v_B = k_B^{on}[B][H^+] - k_B^{off}[BH^+] \quad (4b)$$

where $k^{on}$ and $k^{off}$ are the binding and unbinding rate constants.

The permeation fluxes of propionate ($j_{AH}$) and TMA ($j_B$) are described as:

$$j_{AH} = P_{AH}\left([AH]_o - [AH]\right) \quad (5a)$$

$$j_B = P_B\left([B]_o - [B]\right) \quad (5b)$$

where $[AH]_o$ and $[B]_o$ are the concentrations in the bath solution.

## Results

Whole-cell patch-clamped neurons, loaded with the pH-sensitive dye (HPTS), were depolarized for 2 s to a range of potentials at 1 min intervals (see Fig. 1a). The regions from which fluorescence was recorded and the neuronal morphology are shown in Fig. 1b. Ratiometric recordings of the pH-sensitive fluorescence showed that depolarization gave rise to a $pH_i$ gradient. Although the regional pH-sensitive fluorescence measurements were ratiometric and calibrate for absolute $pH_i$, when calibrated they showed a

small, fixed (~0.05 pH unit) offset that was independent of manoeuvres that are expected to abolish pH gradients, such as the superfusion of mobile, membrane-permeant pH buffers (Table 2). We, therefore, believe that these offsets are calibration artefacts and we removed them by subtraction, to allow the dynamic $pH_i$ gradients to be analyzed. Hence, we report pH shifts on a relative scale with an indication of the mean starting calibrated $pH_i$ value. Depolarization to 0 mV evoked an acid shift in 29 out of 43 neurons, although depolarization to more positive potentials evoked alkaline shifts of progressively increasing magnitude in all neurons used. As expected from the surface-to-volume ratio, the pH shifts recorded in the axonal regions were always larger than in the soma [4] giving rise to a $pH_i$ gradient. The recovery of regional $pH_i$ shifts, after depolarization, is described well by single exponentials. Exponentials fitted to such pH data, using the least squares method, are shown in Fig. 1a. The difference between soma $pH_i$ and axonal $pH_i$ during recovery from the $pH_i$ shifts (the longitudinal $pH_i$ gradient) was also calculated and fitted with a single exponential function (Fig. 1c). The first two acidic shifts in Fig. 1a produced $pH_i$ gradients that recovered with time constants of 12.9 s (0 mV depolarization) and 15.1 s (+20 mV depolarization). The +60 mV depolarization produced an alkaline shift with a $pH_i$ gradient that recovered with a time constant of 17.1 s. Although depolarization to +60 mV was associated with some delayed calcium-dependent acidification [4], seen in the soma trace, this did not appear to markedly accelerate the collapse of the $pH_i$ gradient as judged by the time constant. Hence, we performed all subsequent analysis on pH shifts evoked by depolarization to +60 mV as they were both large and robust.

Figure 2 shows the average exponential parameters used to fit the pH recoveries for axonal and soma regions as well as for the gradient. In Fig. 2a, it can be seen that the axonal pH recovery occurs approximately three times faster than that in the soma. In addition, Fig. 2b shows that the alkaline transient was also approximately three times larger in the axon than in the soma. The longitudinal $pH_i$ gradient fits were dominated by the axon exponentials as they were both larger and faster.

Such mean data do not, however, take into account the wide range of different dimensional characteristics of

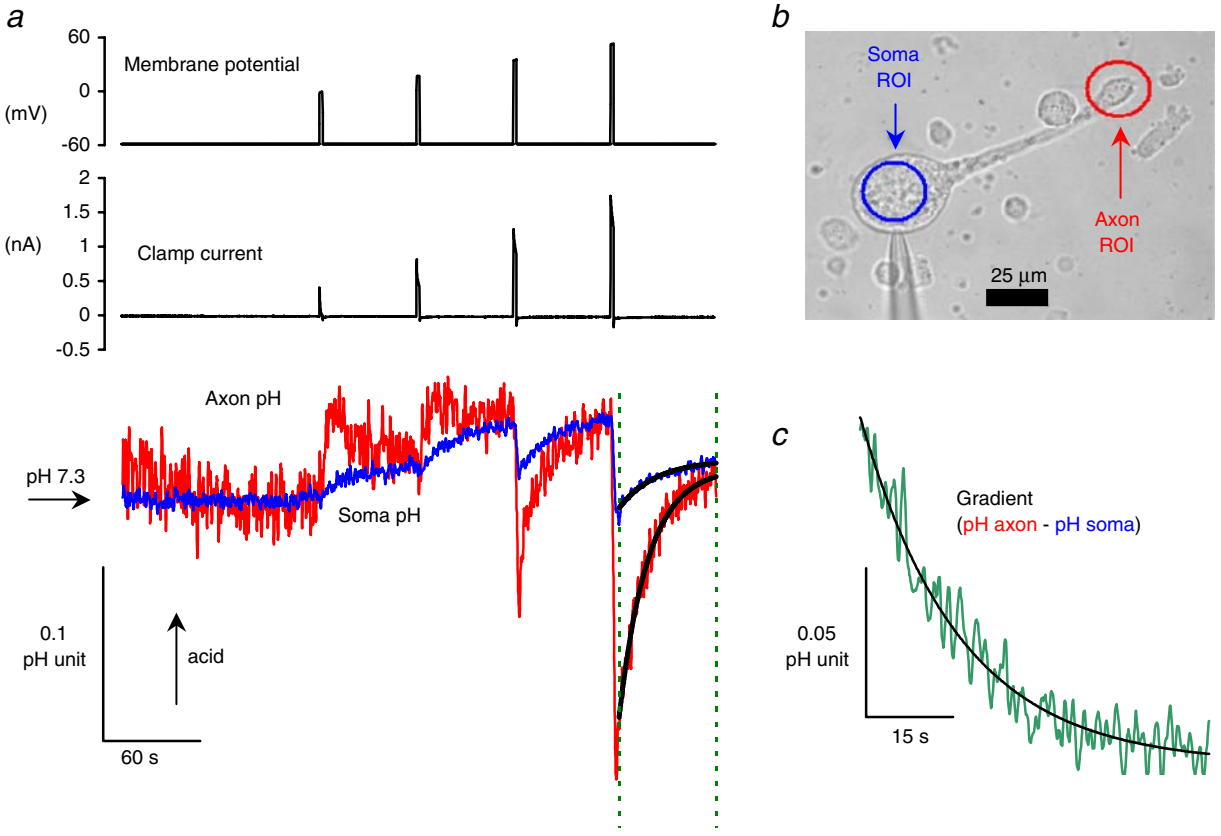


**Fig. 1** Ratiometric recording of soma and axonal pH from an isolated snail neuron, showing effects of four depolarizations. **a** Records of membrane potential, clamp current and regional $pH_i$ (plotted with acidifications as upward deflections) during depolarization to 0, +20, +40 and +60 mV for 2 s. The regional $pH_i$ traces have been offset (soma ~0.1 pH unit) to remove any apparent steady-state pH difference (see Materials and methods). Axon and soma $pH_i$, 60 s of data after +60 mV depolarization, were fitted by exponentials (axon $\tau$ 16 s and soma $\tau$ 20 s). This experiment is representative of 27 other similar experiments in which these depolarizations were performed. **b** Videomicrograph of the patch-pipette and snail neuron from which data plotted in (**a**) was recorded. The *circles* show the regions from which fluorescence was recorded. **c** Plot of the $pH_i$ gradient (axonal $pH_i$–soma $pH_i$) for 60 s after depolarization to +60 mV, marked by *dotted lines* in (**a**) $\tau$ 15.5 s)

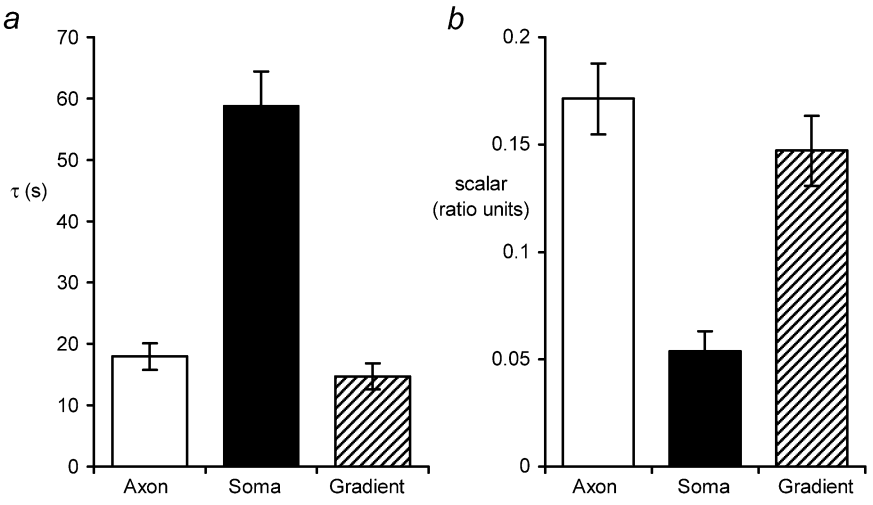


**Fig. 2** Mean data for the exponential recovery times and sizes of $pH_i$ transients evoked by depolarization to +60 mV for 2 s. **a** The exponential time constants (fitted by least squares) for axonal, soma and gradient $pH_i$ recoveries (mean±SEM, $n$=28 for axon and gradient, $n$=27 for soma). **b** The size of the axonal, soma, and gradient $pH_i$ shift, calculated from the exponential fit (mean±SEM, $n$=28 for axon and gradient, $n$=27 for soma)

known snail neuronal morphology [32]. These dimensions might be expected to play an important role in shaping the kinetics of a diffusional process [12].

In Fig. 3, we have categorized three of these dimensional variables and the relationships between them. Figure 3a illustrates the measurements of axon length, axon diameter and soma diameter. Mean data for the 26 isolated snail neurons from which dimensional measurements were made are (mean±SD) axon length 60±24 μm, axon diameter 6.2±2.7 μm and soma diameter 33±9.0 μm (standard deviation, rather than SEM, is used here to describe the range of sizes within the population).

In Fig. 3b–d we examined whether or not the neurons showed any relationship between these three dimensions. Axon length (Fig. 3b,c) did not significantly correlate with either axon or soma diameter, as would be expected from an isolation procedure that severs the axon at random points. There was, however, a correlation ($P$<0.001) between axon and soma diameter (Fig. 3d) with the axon diameter being on average 39% of the soma diameter.

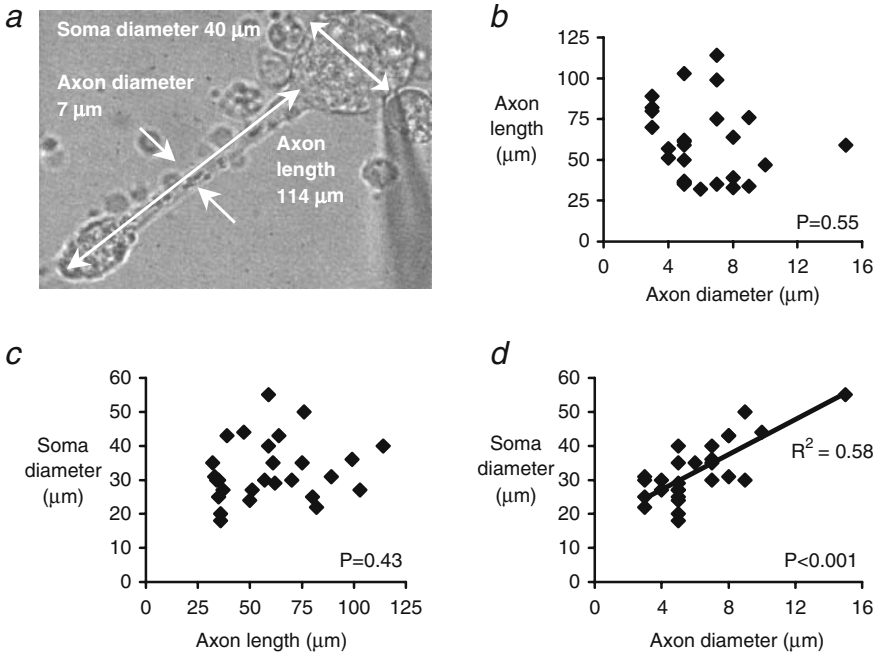


**Fig. 3** Relationships between axon diameter, axon length and soma diameter for isolated snail neurons. **a** Videomicrograph of a patch-clamped snail neuron illustrating the size measurements made. Axon length was measured from the cell body to the axon tip. Axon diameter was measured at the mid-point of the axonal length. The soma diameter was measured through the diameter perpendicular to the long axis of the axon. **b** Plot of axon length against axon diameter from 26 neurons. Linear regression analysis showed no significant relationship between these two parameters ($P$=0.55). **c** Plot of soma diameter against axon length ($n$=26). Linear regression analysis showed no relationship between the two dimensions ($P$=0.43). **d** Plot of soma diameter against axon diameter ($n$=26). A significant positive correlation ($P$<0.001) was found between these two variables. The least squares fitted line has a slope of 2.6 and a theoretical $y$-axis intercept of 16.8 μm ($r^2$ 0.58)

In Fig. 4a, we have plotted the time constants for the recovery from alkaline loads against axon length. Longer axon lengths are associated with significantly ($P$<0.001) slower recoveries from the alkaline load. Such a relationship might be expected if the recovery involved the diffusion of protons along the axon. There was no systematic correlation between the size of the axonal pH shift and the axon length (Fig. 4b), nor was there between the axon time constant and the axon diameter (Fig. 4c). However, the size of the pH shift in the axon was related ($P$<0.005) to the axon diameter with large shifts occurring in smaller-diameter axons (Fig. 4d).

Although the time constant for the recovery of the axonal pH transient is related to axonal length, in vivo the presence of membrane-permeant weak acids and bases might be expected to interfere with this relationship. The presence of weak acids and bases would be expected to have complex effects on the pH gradients. Although such open-buffer systems [25] would be expected to reduce the size of pH gradients, it is not clear what effect they would have on the time course of their collapse. The increased buffering power might slow the return of a uniform pH since greater numbers of $H^+$ would have to diffuse; however, facilitated diffusion along the axon might more than compensate for this effect.

To test the effect of weak acid/base on the pH gradient time course, we applied a weak acid (propionate) and a weak base (TMA) simultaneously—thus avoiding the pH change which would be induced by the application of the weak acid or base on its own. The molar ratio of TMA and propionate in the mix was chosen so as to induce, on average, little change in $pH_i$ ([23] see Materials and methods). We used seven different total buffer concentrations with this property, ranging from 1.88 to 34.0 mM.

Figure 5 shows an example of such an experiment in which we used 7.5 mM propionate and 1.0 mM TMA as the buffer mix. The cell was depolarized to a range of potentials whilst regional $pH_i$ was recorded. Application of the buffer mix caused a small transient alkalinization followed by a sustained acidification of ~0.1 pH units. This acidification was expected since the pH of the cell in the control solution (calculated from the in vitro calibration) was found to be 7.13 while the buffer mix solution had a calculated null pH of 7.06. The series of depolarizations in the presence of the buffer mix resulted in alkaline pH transients which were similar in size, but recovered more rapidly than in the absence of the buffer. Removal of the buffer mix produced a complex change in regional $pH_i$. In the soma, there was an early acidification followed by an alkalinization. In the axon, however, the early acidification was almost absent and there was a pronounced alkalinization. Subsequent depolarization to a range of potentials produced slightly larger axonal alkaline transients compared with both the initial control and the changes in the buffer mix (this was seen in 30 of the 58 experiments performed with weak acids and bases, whilst in 25 experiments, the pH transients became smaller). In Fig. 5c, we show the $pH_i$ gradients on depolarization to +60 mV in the presence and absence of the buffer mix. In the presence of the buffer (trace II), the pH gradient collapses almost three times faster than in the absence of added buffer (trace I).

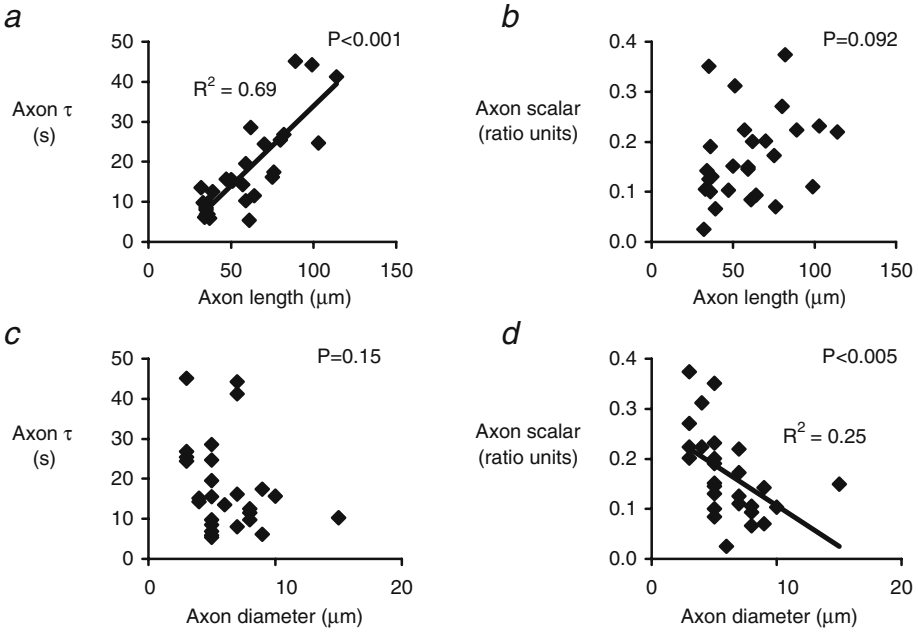


**Fig. 4** Relationships between axonal pH transient kinetics and axonal dimensions. **a** Axonal time constants plotted against axon length ($n$=26) shows a significant positive correlation ($P$<0.001). The least squares fitted line has a slope of 0.40 s $\mu m^{-1}$ with a theoretical $y$-axis intercept of −6.0 s ($r^2$ 0.69). **b** Axonal $pH_i$ shift size plotted against axon length. These two parameters showed no significant correlation ($P$=0.092). **c** Axonal time constant plotted against the axon diameter ($n$=26). These two parameters showed no significant correlation (P=0.15). **d** Axonal pH shift size plotted against axon diameter ($n$=26). These two parameters showed a significant correlation ($P$<0.005). The least squares fitted line has a slope of −0.016 ratio units $\mu m^{-1}$ and a theoretical $y$-axis intercept of 0.27 ratio units ($r^2$ 0.25)

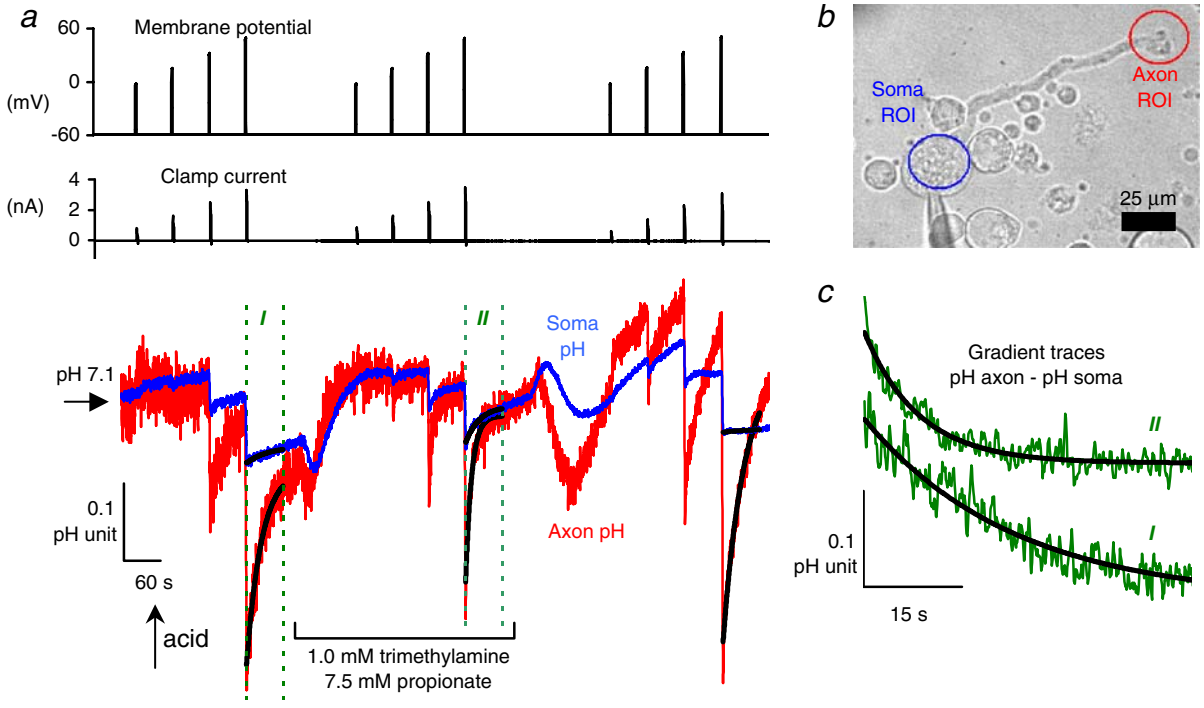


**Fig. 5** The effect of a weak acid/base buffer mix on axonal and soma pH transients evoked by depolarization. **a** Traces of membrane potential, clamp current and regional intracellular $pH_i$ during depolarization and the addition of 1.0 mM TMA and 7.5 mM propionate. The recoveries of pH shifts from depolarization to +60 mV were fitted with exponentials. In the absence of added weak acid/base, the axonal τ were 24.7 and 32.1 s whilst the soma τ were 73.4 and 100 s. During superfusion with the TMA/propionate mix, the axonal τ fell to 9.4 s and the soma τ to 16.1 s. The $pH_i$ gradients between the two sections, delineated by *dotted lines* (marked *I* and *II*), are shown in (**c**). This experiment is representative of a total of six experiments made with these buffer concentrations, and depolarizations. **b** Videomicrograph of the snail neuron from which the recordings were made in (**a**). **c** The $pH_i$ gradients after depolarization to +60 mV from the sections *I* and *II* in **a**. The time constants were 23.2 s in the absence of added buffer and 8.4 s in the presence of the buffer mix

Mean data for the effects of total buffer concentrations on transient kinetics are shown in Fig. 6. Figure 6a shows the effect of buffer concentration on the soma and axonal pH time constants. An increase in total buffer concentration produces an exponential decline in the time constant for the decay of the local $pH_i$ shifts in both the soma and the axon. This exponential relationship indicates that even small amounts of additional mobile buffer are able to greatly reduce the time taken for pH gradients to dissipate. However, the data presented in Fig. 6a were produced from neurons with varied axonal length. Thus, at least some of the scatter within the data sets must result from axon length differences. In Fig. 6b, we show data for the time constants of axonal pH recovery after alkaline load from four neurons with different axonal lengths, using a total of 22 mM buffer. The effect of the weak acid base mix was to speed the pH recovery from the alkaline load in proportion to the axon length. This result is consistent with the buffer mix acting over the entire length of the axon to speed pH recovery.

In Fig. 6c, we show the relationship between the size of the pH shift and the concentration of added buffer. The effect of additional intracellular $H^+$ buffering power provided by the weak acid and base should theoretically be much greater than the observed effect on the $pH_i$ transients. However, the data plotted in Fig. 6c is from dynamic pH transients which are unlikely to conform to steady-state predictions. Firstly, the buffer mix is unlikely to diffuse fast enough to act in a totally open fashion and, secondly, the size of the alkaline load depends upon the rate of proton delivery to and from the channel.

Although the buffer mix accelerated the collapse of the longitudinal pH gradients, the mechanism of action is not clear. There appear to be two main inter-connected processes by which the acceleration could have occurred. Firstly, the buffer mix could partially recover pH by facilitating the movement of acid equivalents across the cell membrane (i.e. moving from near-instantaneous closed-system buffering to the much more powerful open-system buffering [25]). Such a process of delayed buffering relies on the slow permeation of uncharged buffers. Secondly, it could accelerate the movement of $H^+$ along the axon (facilitated diffusion). These processes are inextricably bound as the formation of a pH gradient in the presence of a weak acid and a weak base causes many longitudinal and transmembrane gradients to form. For instance, both the protonated and unprotonated forms of the weak acid (HA and $A^-$) and the protonated and unprotonated forms of the weak base ($BH^+$ and B) form gradients along the cell as well as across the cell membrane when pH changes. As a result of these gradients, fluxes of HA, $A^-$, $BH^+$, B and $H^+$ occur along the axon and across

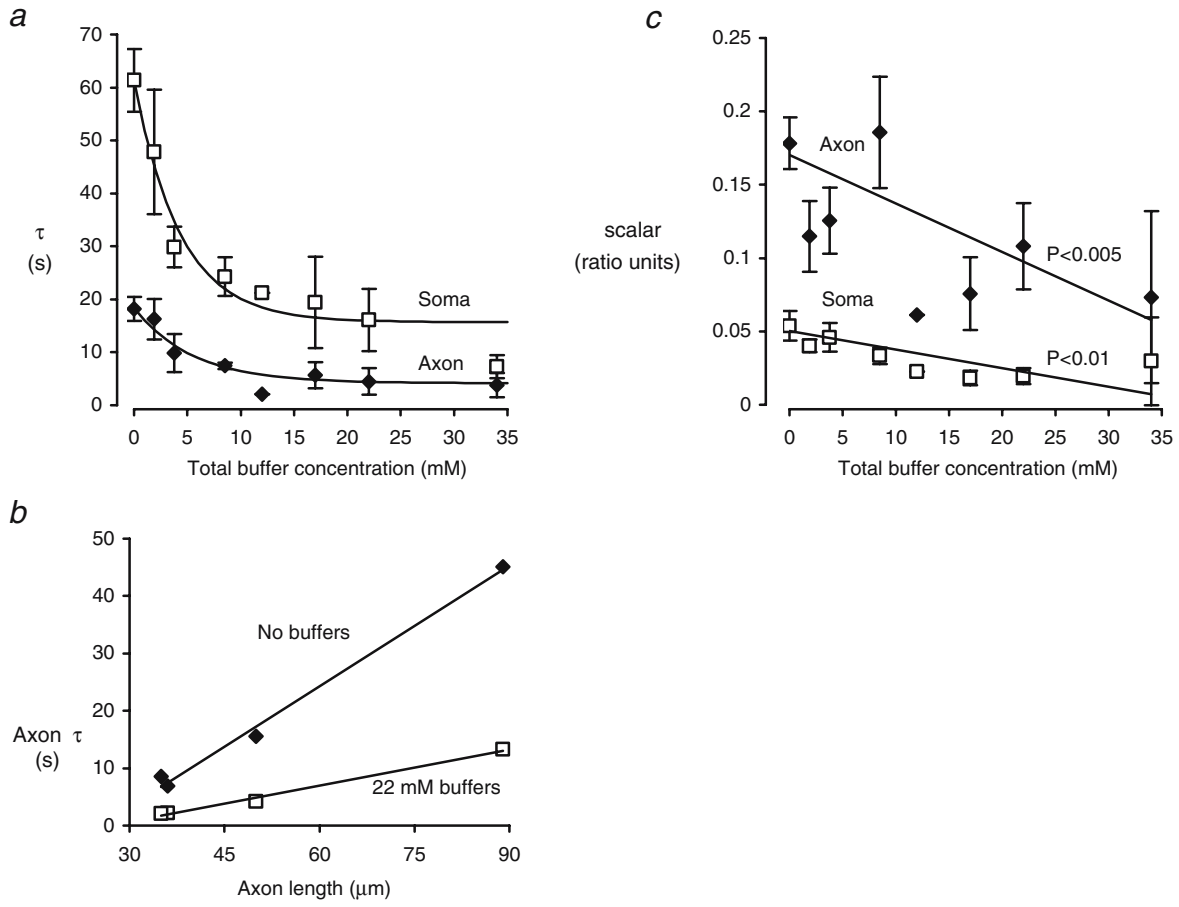


**Fig. 6** The effect of varying total weak acid/base concentration on the kinetics of regional $pH_i$ transients after depolarization to +60 mV (*error bars* show±1 SEM). **a** Plot of exponential time constant for $pH_i$ in the axon and soma against total concentration of weak acid and base in the superfusing solution. Raw data sets were fitted with exponentials (τ axon 5.3 mM and τ soma 4.0 mM). **b** Axonal time constant for the $pH_i$ recovery against axon length in the absence and presence of 20 mM propionate/2.0 mM TMA ($n$=4). Least squares fitted lines show a significant ($P$<0.05) correlation between the time constants and axon lengths in the presence (slope 0.21 s $\mu m^{-1}$, $y$-axis intercept 5.6, $r^2$=0.99) and absence (slope 0.70 s $\mu m^{-1}$, $y$-axis intercept 18 s, $r^2$=0.99) of the buffer mix. **c** Plot of pH transient size for the $pH_i$ shift in the axon and soma against total buffer mix concentration. Raw data sets were fitted with *straight lines* (axonal slope −0.0031 ratio units $mM^{-1}$, $y$-axis intercept 0.16 ratio units ($P$<0.005); soma slope −0.0012 ratio units $mM^{-1}$, $y$-axis intercept 0.05 ratio units ($P$<0.01))

the membrane such that the fluxes along the axon are altered by the transmembrane fluxes and vice versa. Nevertheless, we set out to test whether transmembrane fluxes, which can be broadly thought of as open-system buffering, or longitudinal fluxes of the weak acid/base were the most important recovery mechanism. We did this by attempting to drive the uncharged membrane-permeant species (HA and B) to equilibrium across the membrane (in each region), thus, greatly reducing, at least initially, open-system buffering as a mechanism by which the pH gradient could recover. We drove HA and B towards equilibrium by holding the regional pH constant using long depolarizations. The depolarization period chosen, and therefore also the equilibration period, was longer than the collapse time for the pH gradient in the presence of the weak acid and base. The results are presented in Fig. 7.

Figure 7a shows the effect of the buffer mix on neurons depolarized for varying lengths of time. The buffer mix caused a small acidification and had the expected effect of speeding the collapse of the pH gradient. However, the depolarization time (2, 4 and 16 s) had no significant effect on the time constant for recovery of the pH gradient both in the absence ($P$>0.17) and presence ($P$>0.30) of the buffer mix (Fig. 7c shows the pH gradients for the different times normalized for comparison). In Fig. 7c, it can be seen that the pH gradient, during the 16-s depolarization in the presence of the buffer mix, was relatively steady for ~10 s. This period should have been long enough to bring the membrane-permeant forms of the weak acid and base into equilibrium across the cell membrane. As the pH gradient collapse time was largely unaffected by this equilibrium, it seems unlikely that simple transmembrane weak acid and base fluxes (open-system buffering) alone could underlie the pH gradient collapse.

Figure 8 shows the mean data for the effect of the propionate/TMA mix on the collapse of $pH_i$ gradients evoked by different lengths of depolarization. The weak acid and base mix accelerated the collapse of the pH gradient irrespective of the depolarization length, indeed it

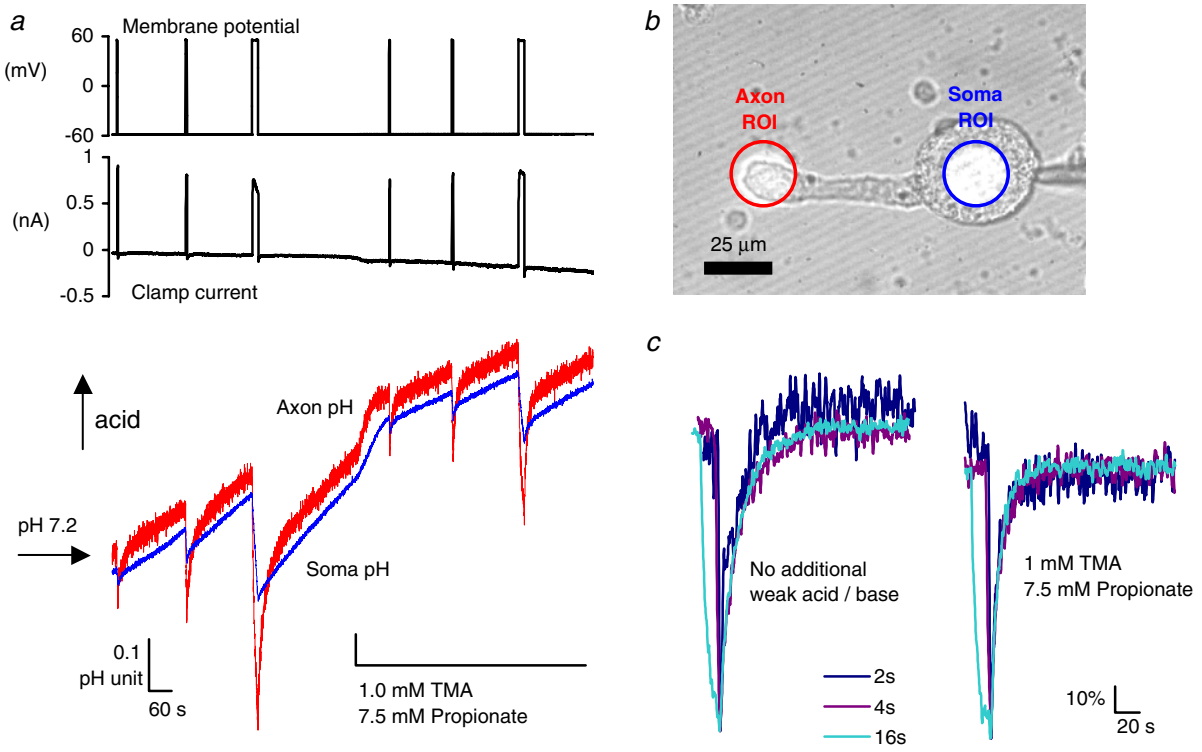


**Fig. 7** Ratiometric recordings of soma and axon $pH_i$ from an isolated snail neuron during depolarization. **a** Records of membrane potential, clamp current and the effect of 1.0 mM TMA/7.5 mM propionate on the recovery of regional $pH_i$ during depolarizations to 60 mV for 2, 4 and 16 s. **b** Videomicrograph of the snail neuron from which the recordings were made in (**a**). **c** Normalized, time-aligned gradient $pH_i$ recoveries for 2-, 4- and 16-s depolarizations to 60 mV in normal Ringer (*left*) and 1.0 mM TMA/7.5 mM propionate (*right*). In HEPES, the time constants for the gradient collapse were 15.8, 12.8 and 13.9 s for the 2-, 4- and 16-s depolarizations, respectively. In 1.0 mM TMA/7.5 mM propionate, the time constants were 5.2, 7.3 and 6.3 s, respectively

appeared to be more effective after longer depolarizations than short ones.

The development of intracellular pH gradients, in the presence of membrane-permeant weak acids and bases, generates at least 12 inter-related gradients that can alter pH: longitudinal and transmembrane gradients of HA, $A^-$, $B^+$, $BH^+$, $H^+$ and endogenous $H^+$ buffers. Thus, it is hard to predict which acid equivalent flux underlies the pH gradient collapse. We have, therefore, developed a simple model that includes these parameters to test the hypothesis that longitudinal acid equivalent fluxes dominate the collapse of pH gradients in the presence of weak acids and bases. Some of the results of this model are shown in Fig. 9. In the absence of added buffers, the model produces a good prediction of the collapse of pH gradients with an apparent diffusion coefficient of 120 $\mu m^2\ s^{-1}$ (Fig. 9a). Adding weak acid and base mix to the model (Fig. 9b) causes the pH gradient to collapse more rapidly, just as is seen in the experimental data (Fig. 5). However, the model also predicts that the pH gradient should transiently change direction. This is not an intuitively obvious result if one only considers the pH gradient to be driving the flow of acid equivalents along the axon. The pH gradient reversal arises from the complex interaction between the transmembrane and longitudinal fluxes of the weak acid and base species. The size of the pH gradient reversal is dependent upon several parameters, including the membrane permeation and diffusion coefficients of the weak acid and base, which are not known with precision. By plotting the regional concentrations of all the weak acid and base species (data not shown), it is apparent that the gradients of the membrane permeant forms (AH and B) reach equilibrium, and then reverse, before the longitudinal $pH_i$ gradient reverses. However, in contrast, the gradients of the membrane-impermeant forms ($A^-$ and $BH^+$) take much longer to reach equilibrium than is suggested by the

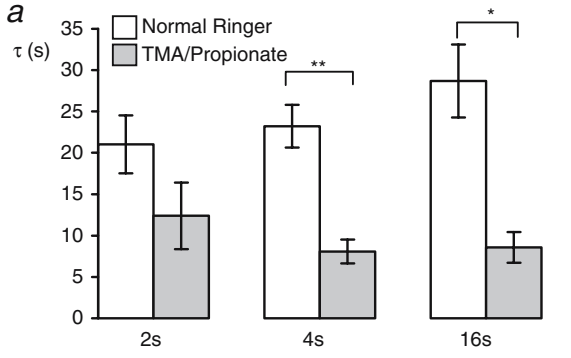


**Fig. 8** Mean time constants for the least-square fit exponentials of $pH_i$ gradients evoked by depolarization to 60 mV for 2, 4 and 16 s. Time constants were significantly faster in the presence of the mixed buffer for the 4-s data ($P<0.001$) and for the 16-s data ($P<0.01$). For the normal Ringer, $n$=14, 16 and 15 for the 2-, 4- and 16-s depolarizations, respectively, and similarly in propionate/TMA, $n$=11, 9 and 7. *$P<0.01$ and **$P<0.001$

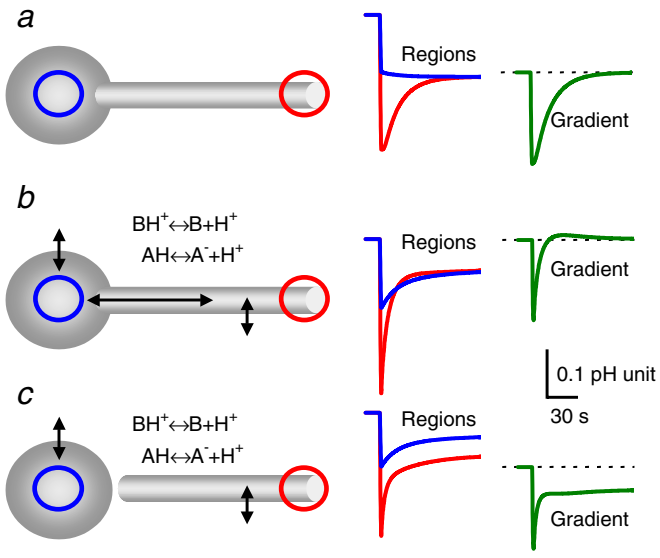


**Fig. 9** Permeation/diffusion model of proton channel-evoked pH transients and gradients in a spherical soma (radius 16.5 m) joined to a cylindrical axon (length 60 μm, radius 3.1 μm). **a** Regional pH changes in the absence of added buffers (see Materials and methods for model description and parameters). **b** pH changes in the presence of 7.5 mM propionate and 1.0 mM TMA. **c** pH changes predicted if there were no diffusion between the axon and soma. In all cases, the bath pH was set as 7.5 and the starting $pH_i$ was 7.1

collapse of the longitudinal $pH_i$ gradient. Thus, in the presence of the weak acid/base mix, the measurement of $pH_i$ alone does not adequately describe the collapse of all of the longitudinal gradients capable of carrying acid equivalents.

Using the model, we can demonstrate the effect of blocking longitudinal acid equivalent diffusion (Fig. 9c). In this case, there is still an initial rapid recovery of the pH gradient, but it is incomplete. This recovery is due to the slow equilibration of HA and B across the membrane and therefore represents the additional $H^+$ buffering of the weak acid and base as it moves from the near-instantaneous closed-system buffering to an open-system buffer. Clearly without a pathway joining the cell body and the axon, this open system buffer cannot cause the complete collapse of the pH gradient.

## Discussion

Isolated snail neurons vary greatly in terms of their soma diameter, axon length and axon diameter [32]. All of these dimensions would be expected to affect depolarization-evoked pH shifts and their subsequent collapse. To investigate the effect of each of these parameters on the collapse, it was important to determine whether or not there was a relationship between these dimensions (Fig. 3). We found a significant positive correlation between soma and axon diameter (Fig. 3d), but no significant correlations for other relationships (Fig. 3b,c). In vivo, most neurons in snail subesophageal ganglia would be expected to have long axons. However, our isolation technique yielded neurons with short axons severed at apparently random lengths with an apparent lack of correlation between measured axon length and the other dimensions.

In this paper, we describe the effect of neuronal axonal dimensions on the collapse of alkaline $pH_i$ gradients evoked by depolarization in snail neurons. We have shown that longitudinal $pH_i$ gradients collapse more slowly in cells with long axons than in cells with shorter axons (Fig. 4). However, we found no significant relationship between axon diameter and the time for collapse of the alkaline longitudinal $pH_i$ gradients. Although wide axons provide a large cross-sectional area, which would be expected to favour rapid collapse, the greater volume also requires the diffusion of more protons. Also, as the depolarizations were not sufficiently long to allow protons to move to thermodynamic equilibrium in the axonal compartment, decreasing axonal diameter, and therefore increasing surface-to-volume ratio, was associated with larger longitudinal $pH_i$ gradients.

The addition of weak acid/base mixes (in proportions calculated to have little effect on resting $pH_i$, see Table 1) accelerated the rate of collapse of the $pH_i$ gradient (Fig. 6a). For short depolarizations, it is difficult to ascertain whether the collapse of the gradient is dominated by $H^+$ diffusion along the length of the axon, or delayed development of the open-system buffering power as the hydrophobic, protonated weak acid or unprotonated weak base attain transmembrane equilibrium. Figure 6b would seem to suggest that diffusion along the axon is important, as the effect of the buffer mix is proportional to the axonal length. If the action of the weak acid/base, on the collapse of the pH gradient, was merely as an open-system buffer, then it should result in the same time constant for the collapse in axons of varying length. The observed effect would only be expected if the buffers were acting along the length of the axon rather than just at either of the two locations from which pH was being measured. Furthermore, it supports the theory that mobile weak acids and bases help collapse—but do not obliterate—$pH_i$ gradients in neurons [12, 33].

The higher the total buffer concentration, the greater the effect on the pH gradient collapse. Increasing the buffer concentration also reduced the size of the depolarization-evoked alkaline shift, although not by as much as expected for an open-system pH buffer, and there are several possible explanations for this. Firstly, the relatively slow permeation of the weak acid/base across the membrane may have prevented the full open-system buffering from being realized. Secondly, the higher proton mobility offered by the mobile buffers may have increased the total $H^+$ efflux through the proton channels.

The propionate/TMA mix is not known to be a substrate for $pH_i$-regulating mechanisms and, by choosing the concentrations appropriately [23], its application can have little effect on steady-state $pH_i$. The buffer mix will, however, increase both the speed of apparent $H^+$ diffusion and the buffering power, thus accelerating the collapse and reducing the size of the evoked $pH_i$ shifts. Longer

depolarizations, however, allow a pseudo steady-state pH to occur. This allows time for equilibration of the weak acid/base mix across the plasma membrane to take place (Fig. 7). If the equilibration period is similar in time to the collapse of the $pH_i$ gradient (~10 s), then it cannot be argued that transmembrane equilibration alone, after repolarization, dominates the $pH_i$ gradient collapse. Thus, the similar time constants for collapse of the $pH_i$ gradients from 2 or 16 s depolarizations (Fig. 8) would seem to rule out the movement of uncharged weak acid or base across the plasma membrane (open-system buffering) as the main explanation for the accelerated $pH_i$ gradient collapse in the presence of the buffer mix. Thus, it would appear that buffer-facilitated proton diffusion dominates pH gradient collapse in snail neurons bathed in membrane-permeant pH buffers. However, our modeling of the collapse of longitudinal $pH_i$ gradients (Fig. 9) produces a rather different result. The model is simple in that it contains only diffusion of $H^+$ and its equivalents, and does not contain any active $pH_i$ regulation. The model suggests that the development of the open-system buffering power alone, without any facilitated proton diffusion (Fig. 9c), could produce the expected speeding of longitudinal $pH_i$ gradient collapse—albeit only a partial collapse to uniformity. The reasons for the discrepancies between the model and the experiments are currently unclear. The model contains many variables that are not known for snail neurons, most importantly the permeation coefficients for the membrane-permeant buffers, the local membrane surface area and volume fraction. The model also makes the counter-intuitive prediction that the $pH_i$ gradient should transiently reverse direction. This appears to result from the diffusion of the weak acid and base along the axon combined with subsequent permeation across the plasma membrane and is, therefore, sensitive to the rates of weak acid and base permeation. The model highlights the difficulties in understanding, intuitively, what is already a greatly simplified system.

There are many factors that would be expected to alter intracellular $pH_i$ recovery in vivo which were not included in our experimental design including complex cytoarchitecture, the presence of the open-buffer system $CO_2/HCO_3^-$ and its effects on buffering and pH-regulating mechanisms, glial cells, metabolic products and other mobile buffers. Many of these might speed proton movements both across the plasma membrane and through the cytosol. Nevertheless, the long axons found in vivo may produce much more slowly collapsing gradients (with time constants in excess of 1 min) than those reported in vitro. This would be particularly likely for acidic $pH_i$ shifts which have been shown to collapse more slowly in vitro than alkaline shifts due to a reduction in the proton diffusion coefficient [8]. The effects of cellular architecture on the generation, maintenance and collapse of intracellular pH gradients reported in this paper are in agreement with conclusions drawn from earlier non-ratiometric experiments [4] as well as mathematical models [12].

All of the snail neurons we isolated had unipolar axons with no bifurcations. More complex neurons, such as mammalian cerebellar Purkinje neurons, which have both long and thin dendritic branches, might be expected to show similarly slow internal proton diffusion. In such cells, transmembrane pH-regulating mechanisms may well dominate the recovery from acid or alkaline loads. Normal cellular function can involve changes in cytoarchitecture, such as dendritic spine movements [34], which may also be associated with changes in the time course of activity-dependent pH changes. Furthermore, drugs that alter intracellular proton mobility such as carbonic anhydrase inhibitors [9, 33] can be used to alter physiological neuronal function [35]. Thus, understanding the processes that determine local pH (transmembrane pH-regulating mechanisms, buffering and diffusion) may form a critical component of models of neuronal dendritic function [36].

In this study on isolated snail neurons with axons as short as 35 μm, we have reported intracellular pH gradients, measured ratiometrically, that took many seconds to collapse. In cells with axons of approximately 100 μm, the $pH_i$ gradient lasted for over 1 min, and even in the presence of a high concentration of mobile buffers, the pH gradient lasted for tens of seconds. The mobile buffer concentrations we used (1.88–34.0 mM) were much higher than those which would occur physiologically (for instance, normal $[CO_2]$ is ~1.1 mM). However, the diffusion of these buffers was not as fast as the theoretical maximum for $CO_2$. From these results, it is clear that proton diffusion along the axon, even when facilitated by high levels of mobile buffers, is too slow to prevent the generation of large intracellular pH differences. Therefore, the control of pH microdomains that will affect synaptic function [37] is likely to be determined by local pH-regulating mechanisms [38] about which little is currently known.

**Acknowledgements** AP was supported by a Vacation Studentship from the Wellcome Trust. We thank the MRC for past support, and acknowledge its desire to have funded this work. We also acknowledge the University of Cambridge for consumables funding and Roger Thomas for comments on the manuscript.

## References

1. Meech RW, Thomas RC (1977) The effect of calcium injection on the intracellular sodium and pH of snail neurones. J Physiol (Lond) 265:867–879
2. Ahmed Z, Connor JA (1980) Intracellular pH changes induced by calcium influx during electrical activity in molluscan neurones. J Gen Physiol 75:403–426
3. Schwiening CJ, Kennedy HJ, Thomas RC (1993) Proton transport by the plasma membrane $Ca^{2+}$–ATPase of voltage-clamped snail neurones in isolated ganglia. J Physiol 473:39P
4. Schwiening CJ, Willoughby D (2002) Depolarization-induced pH microdomains and their relationship to calcium transients in isolated snail neurones. J Physiol 538:371–382
5. Willoughby D, Schwiening CJ (2002) Electrically evoked dendritic pH transients in rat cerebellar Purkinje cells. J Physiol 544:487–499

6. Thomas RC (1976) The effect of carbon dioxide on the intracellular pH and buffering power of snail neurones. J Physiol (Lond) 255:715–735
7. Abercrombie RF, Hart CE (1986) Calcium and proton buffering and diffusion in isolated cytoplasm from Myxicola axons. Am J Physiol 250:C391–C405
8. Al-Baldawi NF, Abercrombie RF (1992) Cytoplasmic hydrogen-ion diffusion-coefficient. Biophys J 61:1470–1479
9. Spitzer.W, Skolnick RL, Peercy BE, Keener JP, Vaughan-Jones RD (2002) Facilitation of intracellular H+ ion mobility by $CO_2$/$HCO_3^-$ in rabbit ventricular myocytes is regulated by carbonic anhydrase. J Physiol (Lond) 541:159–167
10. Vaughan-Jones RD, Peercy BE, Keener JP, Spitzer KW (2002) Intrinsic $H^+$ ion mobility in the rabbit ventricular myocyte. J Physiol (Lond) 541:139–158
11. Zaniboni M, Swietach P, Rossini A, Yamamoto T, Spitzer KW, Vaughan-Jones RD (2003) Intracellular proton mobility and buffering power in cardiac ventricular myocytes from rat, rabbit, and guinea pig. Am J Physiol Heart Circ Physiol 285: H1236–H1246
12. Swietach P, Zaniboni M, Stewart AK, Rossini A, Spitzer KW, Vaughan-Jones RD (2003) Modelling intracellular $H^+$ ion diffusion. Prog Biophys Mol Biol 83:69–100
13. Dickens CJ, Gillespie JI, Greenwell JR (1989) Interactions between intracellular pH and calcium in single mouse neuroblastoma (N2A) and rat pheochromocytoma cells (PC12). Q J Exp Physiol 74:671–679
14. Seksek O, Bolard J (1996) Nuclear pH gradient in mammalian cells revealed by laser microspectrofluorimetry. J Cell Sci 109 (1):257–262
15. Masuda A, Oyamada M, Nagaoka T, Tateishi N, Takamatsu T (1998) Regulation of cytosol–nucleus pH gradients by $K^+/H^+$ exchange mechanism in the nuclear envelope of neonatal rat astrocytes. Brain Res 807:70–77
16. Ro H, Carson JH (2004) pH microdomains in oligodendrocytes. J Biol Chem 279(35):37115–37123
17. Willoughby D, Thomas RC, Schwiening CJ (1999) A role for $Na^+/H^+$ exchange in pH regulation in *Helix* neurones. Pflugers Arch 438:741–749
18. Thomas RC, Meech RW (1982) Hydrogen ion currents and intracellular pH in depolarised voltage-clamped snail neurones. Nature (Lond) 299:826–828
19. Trapp S, Luckermann M, Kaila K, Ballanyi K (1996) Acidosis of hippocampal-neurons mediated by a plasmalemmal $Ca^{2+}/H^+$ pump. Neuroreport 7:2000–2004
20. Thomas RC (1977) The role of bicarbonate, chloride and sodium ions in the regulation of intracellular pH in snail neurones. J Physiol 273:317–338
21. Schwiening CJ, Boron WF (1994) Na-dependent $Cl^-$–$HCO_3^-$ exchange regulates intracellular pH in freshly isolated pyramidal neurones from the rat hippocampus. J Physiol (Lond) 475:59–67
22. Willoughby D, Thomas RC, Schwiening CJ (1998) Comparison of simultaneous pH measurements made with 8-hydroxypyrene-1,3, 6-trisulphonic acid (HPTS) and pit-sensitive microelectrodes in snail neurones. Pflugers Arch 436:615–622
23. Eisner DA, Kenning NA, O'Neill SC, Pocock G, Richards CD, Valdeolmillos M (1989) A novel method for absolute calibration of intracellular pH indicators. Pflugers Arch 413:553–558
24. Swietach P, Vaughan-Jones RD (2005) Relationship between intracellular pH and proton mobility in rat and guinea-pig ventricular myocytes. J Physiol (in press)
25. Roos A, Boron WF (1981) Intracellular pH. Physiol Rev 61: 296–434
26. Pantazis A, Schwiening CJ (2002) The effect of mobile hydrogen ion buffers on proton channel-evoked pH gradients in *Helix aspersa* neurones. J Physiol 539:13P
27. Grynkiewicz G, Poenie M, Tsien RY (1985) A new generation of $Ca^{2+}$ indicators with greatly improved fluorescence properties. J Biol Chem 260:3440–3450
28. Thomas R, Pagnotta S, Nistri A (2003) Whole-cell recording of intracellular pH with silanized and oiled patch-type single or double-barreled microelectrodes. Pflugers Arch 447(2):259–265
29. Bock G, Marsh J (1988) Proton passage across cell membranes, 1st edn. Wiley, Sussex, UK
30. Marcaggi P, Coles JA (2000) A Cl(−) cotransporter selective for NH(4)(+) over K(+) in glial cells of bee retina. J Gen Physiol 116:125–142
31. Szatkowski MS, Thomas RC (1989) The intrinsic intracellular $H^+$ buffering power of snail neurones. J Physiol (Lond) 409: 89–101
32. Kerkut GA, Lambert JD, Gayton RJ, Loker JE, Walder RJ (1975) Mapping of nerve cells in the suboesophageal ganglia of *Helix aspersa*. Comp Biochem Physiol A 50:1–25
33. Stewart AK, Boyd CA, Vaughan-Jones RD (1999) A novel role for carbonic anhydrase: cytoplasmic pH gradient dissipation in mouse small intestinal enterocytes. J Physiol 516:209–217
34. Majewska A, Tashiro A, Yuste R (2000) Reulation of spine calcium dynamics by rapid spine motility. J Neurosci 20(22): 8262–8268
35. Bain PG, O'Brien MD, Keevil SF, Porter DA (1992) Familial periodic cerebellar ataxia: a problem of cerebellar intracellular pH homeostasis. Ann Neurol 31:147–154
36. Nimchinsky EA, Sabatini BL, Svoboda K (2002) Structure and function of dendritic spines. Annu Rev Physiol 64: 313–353
37. Tombaugh GC (1998) Intracellular pH buffering shapes activity-dependent $Ca^{2+}$ dynamics in dendrites of CA1 interneurons. J Neurophysiol 80:1702–1712
38. Cooper DS, Saxena NC, Yang HS, Lee HJ, Moring AG, Lee A, Choi I (2005) Molecular and functional characterization of the electroneutral $Na/HCO_3$ cotransporter NBCn1 in rat hippocampal neurons. J Biol Chem 280:17823–17830